



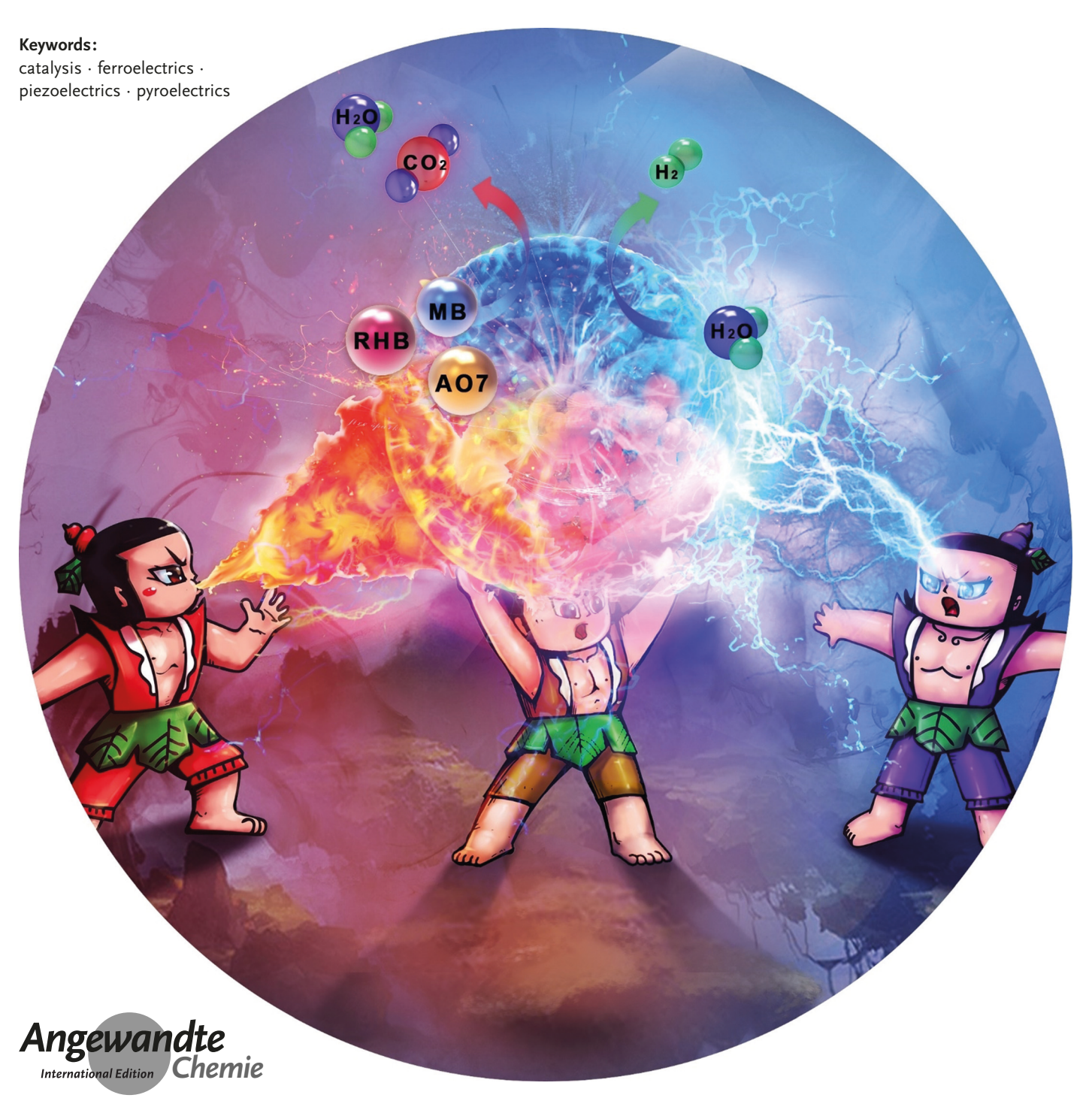


Nanocatalysis

International Edition: DOI: 10.1002/anie.201811709
German Edition: DOI: 10.1002/ange.201811709

Enabling PIEZOpotential in PIEZOelectric Semiconductors for Enhanced Catalytic Activities

Mengye Wang,* Biao Wang, Feng Huang, and Zhiqun Lin*







The past several decades have witnessed significant advances in the synthesis and applications of PIEZOelectric semiconductors, an important class of materials, including piezoelectric, pyroelectric, and ferroelectric semiconductors. The intriguing combination of physical and chemical phenomena in PIEZOelectric semiconductors has triggered much interest in PIEZOcatalysis, that is, catalysis enabled by PIEZOpotential (i.e., piezopotential, pyropotential, and ferropotential)-induced built-in electric fields, which is the focus of this Minireview. First, the PIEZOelectric materials are briefly introduced. Second, recent developments in PIEZOcatalysis are highlighted, including the introduction of representative PIEZOelectric semiconductors, their possible catalytic mechanisms, novel techniques to produce their PIEZOelectric effects during the catalytic process, and several examples of PIEZOcatalysis. Finally, the challenges in the field and exciting opportunities to further improve the PIEZOcatalytic efficiency are discussed.

1. Introduction

Motivated by increasingly serious pollution and depletion of fossil fuels, it is of great importance to convert various forms of renewable energy, such as solar, wind, tidal, and geothermal energy, into applicable and storable chemical energy. Clearly, one strategy is to harvest energy by converting abundant chemicals or pollutants on the earth through catalysis into molecules such as H_2 and CH_4 for use as fuels. The other involves the catalytic degradation of pollutants by capitalizing on sustainable energy, in which the heat- (e.g., geothermal) and strain- (e.g., wind and tide) enabled PIEZOelectrics have been utilized in catalysis.

PIEZOelectrics materials are a class of materials with non-centrosymmetric structure, which are capable of enhancing electrochemical or photochemical processes in response to mechanical deformation. They comprise three subsets of materials, that is, piezoelectric, pyroelectric, and ferroelectric materials (Figure 1). The five capital letters are used in PIEZOelectrics, representing three categories of materials noted above, to differentiate it from the specified piezoelectric materials referring to only one category. As illustrated

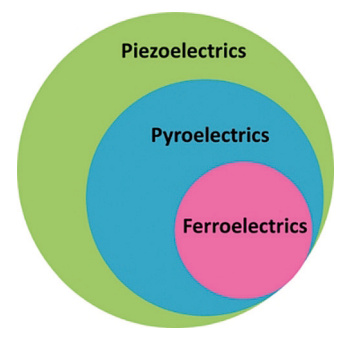


Figure 1. PIEZOelectric materials are composed of piezoelectric, pyroelectric, and ferroelectric materials. Piezoelectric materials contain pyroelectric materials, which in turn include ferroelectric materials.

in Figure 1, piezoelectrics contain pyroelectrics, and pyroelectrics comprise ferroeletrics. Some piezoelectric materials (green) are non-pyroelectric. They experience a separation between positive and negative charge centers upon strain, while exhibiting zero electric dipole in the absence of strain (Figure 2). Partial pyroelectric materials (blue, Figure 1) that are not ferroelectric exhibit spontaneous polarization even under no mechanical deformation (Figure 5). When subjected to strain and changes in temperature, the dipoles of pyroelectric materials change. Ferroelectric materials (pink, Figure 1), which are also pyroelectric and piezoelectric, show polarized electric dipoles without strain and temperature changes. The electric field created inside ferroelectrics by strain, temperature, external electric fields,

or spontaneous existence can significantly influence the electrical environment both inside and around the materials.

The catalytic performance of piezoelectric materials has garnered considerable attention since their breakthrough in 1970s.^[5] The internal electric field arising from the polarization of piezoelectric materials was reported to enhance the separation of charge carriers, leading to improved catalytic properties. [6] In addition, spatial separation of charge carriers was found to impart oxidation and reduction reactions occurring at different sites, reducing the occurrence of the reverse reaction.^[7] DFT calculations showed that the built-in electric field also mediates the adsorption and desorption of reactants and products on the surface of piezoelectric catalysts, which is conducive to overcoming some fundamental limitations on catalysis caused by the Sabatier principle.^[8] Moreover, piezoelectric polarization was also reported to tune the catalytic rate by effectively adjusting the barrier height of a heterogeneous semiconductor interface.^[9]

This Minireview highlights recent development in PIE-ZOpotential-enabled catalysis that capitalizes on piezoelectric, pyroelectric, and ferroelectric semiconductors. We summarize the recent development of PIEZOelectric semiconductors, their PIEZOpotential-mediated catalytic mechanism, special techniques to tailor their piezoelectric proper-

[*] Prof. Dr. M. Wang, B. Wang, Prof. Dr. F. Huang

State Key Laboratory of Optoelectronic Materials and Technologies, School of Materials, Sun Yat-Sen University

Guangzhou 510275 (China)

E-mail: wangmengye@mail.sysu.edu.cn

Prof. Dr. Z. Lin

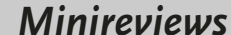
School of Materials Science and Engineering, Georgia Institute of Technology

Atlanta, GA 30332 (USA)

E-mail: zhiqun.lin@mse.gatech.edu

The ORCID identification number(s) for the author(s) of this article can be found under:

https://doi.org/10.1002/anie.201811709.







ties, and some PIEZOcatalytic studies. Finally, the issues and future outlook on the development of PIEZOelectric materials with further enhanced PIEZOcatalytic activities are presented.

2. Piezoelectric-Material-Mediated Catalysis

Piezocatalysis represents a new strategy for enabling or improving the catalytic process by utilizing the strain state of piezoelectric materials.^[10] The piezoelectric effect only exists below the Curie temperature (T_c) . When the temperature T> $T_{\rm c}$, piezoelectric materials lose the piezoelectric property as the spontaneous polarization becomes zero. Non-centrosymmetric metal oxides are ideal candidates for piezoelectric catalysis, including BaTiO₃, $^{[6,11]}$ ZnO, $^{[9,11a,12]}$ PbZr_xTi_{1-x}O₃, $^{[13]}$ ZnSnO₃,^[14] Pb(Mg_{1/3}Nb_{2/3})O₃-32 PbTiO₃ (PMN-PT),^[10,15] MoS₂,^[16] MoSe₂,^[17] BiOIO₃ (or BiOI_{0,926}V_{0,074}O₃),^[18] NaNbO₃,^[19] Bi₄Ti₃O₁₂,^[20] and Bi₂O₂(OH)(NO₃).^[21] The most commonly observed morphologies of the materials employed in piezocatalysis are 1D (e.g., microfiber, $^{[11a,b,13a]}$ nanowire, $^{[11f,12b,14]}$ nanostrip, $^{[18]}$ and nanorod $^{[12f,19,22]}$) and 2D structures (e.g., nanoplatelet, [12e] nanoplate, [18] and nanosheet [21]). It is notable that the deformable morphology of 1D and 2D structures is not a prerequisite for piezoelectric catalysis, as materials of other morphologies (e.g., microsphere, [13b] micropowder, [11c,d] nanoparticle, [11e] nanocube structures, [6] and even hierarchical structures such as nanoflowers composed of nanopetals[16,17] and microspheres assembled from slices or cubes^[20]) are also applicable in piezoelectric catalysis.

The mechanical deformation of piezoelectric materials (that is, not pyroelectric or ferroelectric) induces an electric field that augments the energetics of both free and bound charges throughout the material.^[10] When imposed by mod-

erate to severe strain, piezoelectric materials can generate potentials of tens to hundreds of volts.^[23] Piezoelectric materials that are not ferroelectric show no internal dipole without strain (Figure 2a). When strained, dipole moments are created by the lattice displacement. Compressive and tensile stress produce the polarized electric field of a different

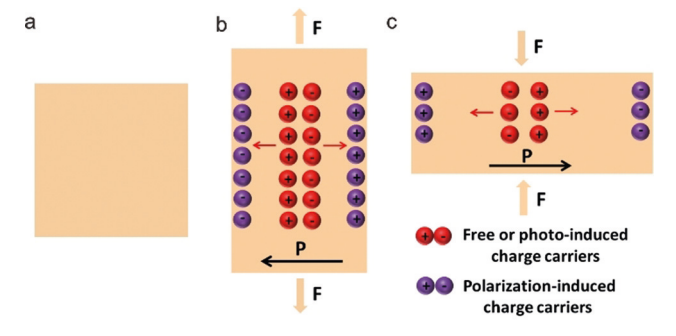
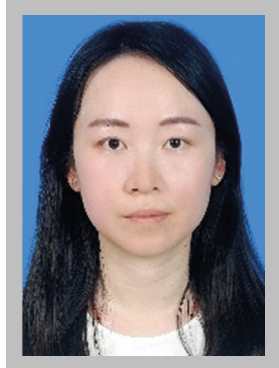


Figure 2. Piezoelectric materials a) without strain, b) under tension, and c) under compression.

direction as shown in Figure 2b and Figure 2c, respectively. Driven by this polarized potential, free electrons and holes or photo-generated ones are separated and forced to move towards the opposite directions (Figure 2b,c). As a result, the recombination of charge carriers is inhibited, and more electrons and holes reach the active sites on the surface of catalysts for the redox reaction.

Several methods have been utilized to exert mechanical strain on piezoelectric materials. For instance, stress was introduced on ZnO monocrystalline nanoplatelets by cooling the hybrid ZnO/TiO₂ nanoplatelet catalysts from high to room temperatures.^[12e] As the thermal expansion coefficients



Mengye Wang is an Associate Professor in the School of Materials at Sun Yat-Sen University. She received her PhD in physical chemistry from Xiamen University in 2015. Her research interests include advanced materials for environmental and energy-related applications, such as photocatalysis, electrocatalysis, and dye-sensitized solar cells.



Feng Huang is a Professor in the School of Materials at Sun Yat-Sen University. He received his PhD in condensed matter physics from the Institute of Physics, Chinese Academy of Sciences in 1999. His research interests include nanocrystalline science, materials science, chemical synthesis, and condensed matter physics.



Biao Wang is pursuing his PhD in condensed matter physics from Sun Yat-Sen University. He obtained his B.S degree from the University of Chinese Academy of Sciences in 2017. His current research focuses on advanced materials for photocatalysis and electrocatalysis.



Zhiqun Lin is a Professor in the School of Materials Science and Engineering at the Georgia Institute of Technology. He received his PhD in polymer science and engineering from the University of Massachusetts, Amherst in 2002. His research interests include perovskite solar cells, polymer solar cells, photocatalysis, electrocatalysis, batteries, thermoelectrics, organic—inorganic semiconductor nanocomposites, quantum dots (rods), conjugated polymers, block copolymers, polymer blends, hierarchical structure formation, and assembly.





of ZnO and TiO2 are largely different, the mismatched thermal expansion coefficients created a residual strain.^[12e] Interestingly, a stirring process was employed to induce compression on PbZr_xTi_{1-x}O₃.^[13b] Moreover, the stirring speed was found to significantly influence the catalytic reaction.^[13b] When the stirring speed increased from 200 rpm to 900 rpm, the degradation efficiency of rhodamine B (RhB) increased from 10% to 37%, [13b] which was attributed to the higher built-in electric field induced by the higher stirring speed.^[13b] Mechanically brushing/sliding was also employed to impose the force. [12b] For example, ZnO nanowires were vertically grown on carbon fibers (CFs), and several bundles of ZnO nanowires/CFs were then woven together to yield the final photocatalytic electrode (Figure 3 a). [12b] When CFs were mechanically pulled, ZnO nanowires moved against each other, and a piezoelectric field across their width was thus formed. [12b] Photo-generated

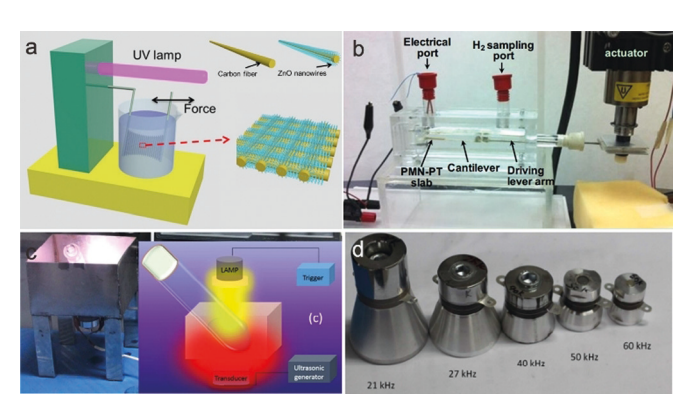


Figure 3. a) Schematic of a device for photocatalytic degradation of a MB solution under UV irradiation in conjunction with periodic mechanical brushing/sliding. Adapted with permission from Ref. [12b]. Copyright 2015, Elsevier. b) An experimental apparatus for piezocatalytic hydrogen evolution. Adapted with permission from Ref. [10]. Copyright 2012, Wiley. c) A piezocatalytic device under ultrasound and light irradiation and d) ultrasonic transducers of different frequencies. Adapted with permission from Ref. [6]. Copyright 2015, American Chemical Society.

electrons and holes were driven by this piezoelectric field and migrated to the opposite side, thereby improving the photocatalytic degradation of methylene blue (MB).[12b] Notably, a special device was designed to study the piezoelectric effect on electrochemical reactions, [10] in which the PMN-PT cantilever coated with gold electrodes was attached to an actuator to generate strain (Figure 3b).^[10]

The most common approach to induce the mechanical is to employ ultrasound irradiation (Figure 3c). [9,12a,b,16a,18] One advantage of this technique is that a high pressure can be applied on the sample. The total pressure consists of the periodic acoustic pressure of ultrasonic waves and the pressure produced by the collapse of the acoustic cavity walls.^[6] Under intense ultrasonic vibration, extraordinarily active bubbles are formed and then collapse, consequently creating a high local pressure (even higher than 100 MPa). [24] The other advantage is that the periodic compression stress caused by ultrasonic waves prevents piezoelectric polarization charges from being fully screened by free carriers or photo-generated carriers. [6] When a static stress is applied on piezoelectric materials, an internal electric field is generated. Free carriers or photo-induced carriers are forced to separate by this built-in electric field, which quickly renders the built-in field to be weakened and eventually diminished by these carriers. However, the ultrasonic wave enables the periodic on/off of the built-in field by using ultrasonic transducers of different frequencies (Figure 3d).^[6] Consequently, during the off state of ultrasonic wave, carriers originally attracted on the surface of piezoelectric catalysts are released, thereby hindering the screening of the built-in field and ensuring the continuous separation of free or photogenerated electrons and holes.^[6]

The piezoelectric effect can be utilized in catalysis (i.e., piezocatalysis) in several different ways. The first way involves the use of free carriers. The polarized electric field is produced to manipulate free carriers of catalysts in the dark.[16a,17,18] It has been demonstrated that the polarized charges do not directly participate in the redox process.^[13b] Wu et al. applied a piezocatalytic effect to separate the free carriers of single and few-layer MoS₂ nanoflowers (NFs) and trigger the degradation of rhodamine B (RhB) in the dark. [16a] The catalytic activity achieved by using MoS₂ NFs under the ultrasonic excitation was much higher than that obtained by using commercial MoS₂ sheets and P25 (Figure 4a).^[16a] The degradation rate of RhB reached 40336 ppm Lmol⁻¹s⁻¹ (i.e., approximately 93% degradation within 60 s), which is the best degradation efficiency ever reported. [16a] During ultrasonic catalysis, polar water molecules were adsorbed onto the polarized surface of MoS₂. Highly active species such as free oxygen radicals, hydroxyl radicals, and hydroperoxyl radicals were thus formed, effectively destroying RhB molecules (Figure 4b).[16a]

As the second way, similar to free carriers, piezoelectric polarization can be used to mediate photo-generated carriers. [19] This piezoelectric effect combines three aspects, that is, piezotronics, piezophotonics, and optoelectronics, in one material, which is referred to as piezophototronic effect by Wang in 2010. [28] Khare et al. reported that the separation rate of photogenerated electron and hole pairs was significantly enhanced under ultrasonic vibration (Figure 4c), resulting in a much higher photocatalytic degradation rate of MB with the ultrasonic piezo-potential manipulation than that without the piezo-electric field (Figure 4d). [19] Huang et al. reported that macroscopic polarization enhancement in BiOIO₃ can efficiently promote the separation of photo-induced charge carriers, leading to the high evolution rate of reactive oxygen species (e.g., hydroxyl radicals and superoxide radicals).^[18] After doping vanadium into the lattice of BiOIO₃ to yield V-BiOIO₃, V⁵⁺ ions replaced I⁵⁺ ions in IO₃ polyhedra, thereby strengthening the polarization of BiOIO3 and further improving the piezophoto-catalytic process.^[18]

The third way invokes the utilization of hybrid catalysts for the piezoelectric effect. [6] For example, the spontaneous polarization potential of BaTiO3 was applied to separate photo-induced carriers of Ag₂O nanoparticles deposited on the surface of BaTiO₃ nanocubes.^[6] With the assistance of periodic ultrasonic waves, an alternating polar charge-created electric field in the BaTiO₃ nanocubes acted as a driving force





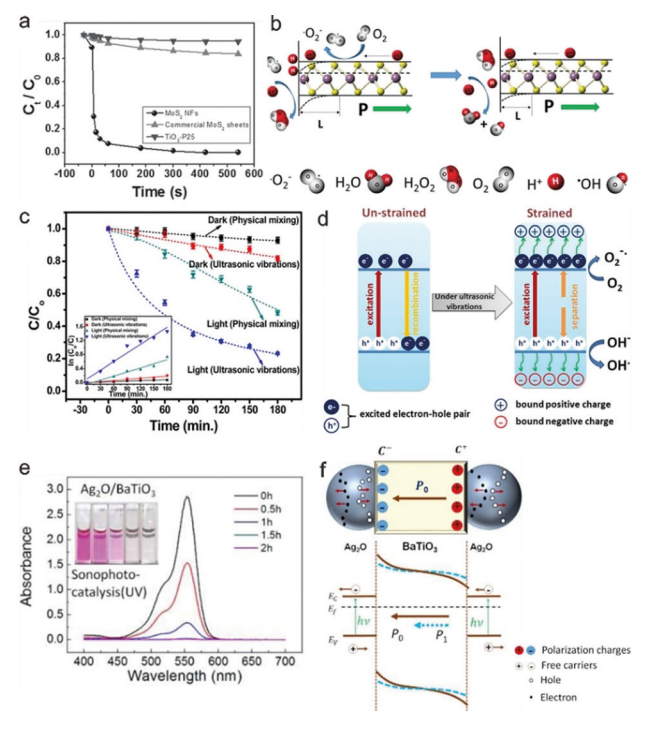


Figure 4. The piezoelectric effect in the separation of free charge carriers: a) Degradation ratio of RhB under ultrasound irradiation in the dark. b) The piezocatalytic process in (a). H⁺ and polar hydroxyl radicals are adsorbed on the surface of MoS₂ with the majority of free carriers (electrons) to produce H_2O_2 . H_2O_2 further reacts with H^+ to yield water molecules and hydroxyl radicals under the internal electric field. (a-b) Adapted with permission from Ref. [16a]. Copyright 2016, Wiley. The piezoelectric effect in the separation of photo-induced charge carriers: c) Photocatalytic degradation of MB under different conditions (under light irradiation or in the dark in conjunction with or without ultrasonic vibration). d) The piezophotocatalytic mechanism of MB degradation by a NaNbO₃ particulate suspension under light and ultrasonic vibration. In the absence of strain, photo-induced charge carriers are easily recombined. Under ultrasonic vibration, the recombination rate of photo-generated electrons and holes is greatly reduced. Thus, more charge carriers migrate to the surface of NaNbO₃ and increase the formation of 'OH and 'O2 radicals. (c-d) Adapted with permission from Ref. [19]. Copyright 2017, Elsevier. Polarized piezoelectric field generated by BaTiO₃ separates photogenerated charge carriers of Ag₂O: e) Absorption spectra of RhB solution under UV and ultrasonic irradiation using Ag_2O -BaTiO $_3$ hybrid materials as catalysts. f) The catalytic mechanism of the process in (e). Photoexcited electrons and holes of Ag₂O nanoparticles move toward the opposite sites induced by the polarization charges of BaTiO₃ nanocubes with a mechanical strain. The solid and dashed line represent the electronic band structure of the BaTiO3 nanocubes without and with the presence of external stress, respectively. e-f) Adapted with permission from Ref. [6]. Copyright 2015, American Chemical Society.

for the separation of electrons and holes in Ag_2O nanoparticles (Figure 4 f), which favored a high photocatalytic activity of Ag_2O –BaTiO₃ hybrid photocatalysts (Figure 4 e). [6] More examples of piezoelectric catalysis are listed in Table 1.

3. Pyroelectric-Material-Mediated Catalysis

Differing from piezoelectric materials discussed above, pyroelectric materials have dipoles even without strain (Figure 5 a). In this class of materials, compressive or tensile strain can change the original dipole polarization (Figure 5 b,c). If the strain is large enough, the polarization will shift to the opposite direction. In addition to strain, the temperature fluctuation also creates the built-in electric field and changes the original polarization inside pyroelectric materials as the temperature variation slightly alters the atom positions in the crystal structure. Clearly, geothermal energy and solar and industrial waste heat can drive the conversion of heat into electricity using pyroelectric materials. The pyroelectric current can be expressed as follows [Eq. (1)]:^[31]

$$I = p \cdot A(dT/dt) \tag{1}$$

where p is the pyroelectric coefficient, A is the electrode area, and dT/dt is the rate of temperature fluctuation. In addition to these parameters, the size of catalysts also affects the pyroelectric current. Nanomaterials usually display higher pyroelectric current than their bulk counterparts owing to the lower defect density. [32]

Figure 6a-d schematically illustrates the pyrocatalytic mechanism. When the pyroelectric catalysts reach thermodynamic equilibrium with its surrounding, polarized carriers are totally screened by compensation carriers from their own free carriers and the surrounding electrolyte (marked as top and bottom blue stripes in Figure 6a).^[29] When the temperature increases, the polarized dipole moments decrease owing to its pyroelectric property.^[29] The thermodynamic equilibrium is broken and the catalysts become less polarized. Consequently, some previously screened carriers in the blue stripes become uncompensated again (Figure 6b). The charged chemical species in the electrolyte (marked with a blue arrow) will thus be adsorbed onto the surface of the catalysts (Figure 6b).^[29] When the temperature remains unchanged, the thermodynamic equilibrium is again formed (Figure 6d). [29] Conversely, under decreased thermal irradiation. the polarized dipole moments increase owing to the heat dissipation from the pyroelectric catalysts (Figure 6c).^[29] The adsorption of chemical species onto the catalysts from the electrolyte takes place again. [29] In addition to favoring the adsorption and desorption of chemical species, more free carriers of catalysts participate in the redox reactions during the changes of the reaction temperature. Consequently, the catalytic performance is largely enhanced during the temperature change.

Benke et al. were the first to verify hydroxyl radicals generated by thermally excited pyroelectric BaTiO₃-Pd nanoparticles, ^[35] uncovering the possible pyrocatalytic mechanism and signifying the potential application of pyroelectric effect in catalysis. A year later, Jia et al. reported the successful pyrocatalytic degradation of RhB, methyl orange (MO), and MB using BiFeO₃ as catalysts. ^[29] The pyroelectric effect was also applied in the disinfection of 2',7'-dichlorodihydrogluorescin (DCFH) with LiNbO₃ and LiTaO₃ particles as catalysts. ^[36] The successful oxidative conversion of DCFH to 2',7'-



Minireviews



Table 1: Comparison of the catalytic performance among various nanostructured piezocatalytic semiconductors.

nanostructured semiconductors	external sources	catalytic applications catalytic performance		Ref.
BaTiO ₃ dendrites	ultrasonic vibration	degradation of AO7 $(c=5.5 \text{ mg L}^{-1})$	$k^{[a]} = 0.0312 \mathrm{min}^{-1}$	
$Pb(Zr_{0.52}Ti_{0.48})O_3 \ fibers$	ultrasonic vibration	degradation of AO7 $(c = 10 \text{ mg L}^{-1})$	$k = 0.00446 \text{ min}^{-1}$	[13a]
Ag ₂ O-BaTiO ₃ hybrid nanocrystals	ultrasonic vibration + UV	degradation of RhB $(c=15 \text{ mg L}^{-1})$	RhB totally degraded within 1.5 h, faster than under UV light only (over 3 h)	[6]
ZnSnO ₃ nanowires	bending stress + UV	degradation of MB $(c=4 \text{ ppm})$	ca. 27% improvement of degradation by piezo- phototronic over piezotronic catalysis	[14]
Ag-ZnO branched heterostructures	ultrasonic vibration + UV/Vis	degradation of MO $(c=13 \text{ mg L}^{-1})$	90% degradation by piezophototronic catalysis within 75 min, less than 20% for photocatalysis	[12a]
ZnO nanowires	mechanical brushing/slid- ing + UV	degradation of MB $(c=5 \text{ mg L}^{-1})$	ca. 100% degradation by piezo-phototronic catalysis within 120 min, 60% for photocatalysis	[12b]
FeS/ZnO nanoarrays	ultrasonic vibration + UV/Vis	degradation of MB $(c=5 \text{ mg L}^{-1})$	97% degradation within 50 min	[12c]
CuS/ZnO nanowires	ultrasonic vibration + UV/Vis	degradation of MB $(c=5 \text{ mg L}^{-1})$	$k = 0.18236 \text{ min}^{-1}$	[12d]
$Ag_2O/tetrapod-ZnO$	ultrasonic vibration + UV	degradation of MB $(c=5 \text{ mg L}^{-1})$	99% degradation within 2 min	[25]
ZnO/TiO ₂ nanoplatelets	thermal stress + UV	degradation of MB $(c = 5 \text{ mg L}^{-1})$	20% improvement of degradation by piezophoto- tronic catalysis over that by photocatalysis	[12e]
$Zn_{1-x}SnO_3$ nanowire arrays	ultrasonic vibration + UV	degradation of MB (c=4 ppm)	$k = 0.015 \text{ min}^{-1}$	[26]
few-layer MoS ₂ nanoflowers	ultrasonic vibration	degradation of RhB (c=10 ppm)	93% RhB degraded within 60 s	[16a]
polydimethylsiloxane-PMN- PT@TiO ₂ film	ultrasonic vibration + UV	degradation of RhB $(c=12 \text{ mg s}^{-1})$	55% improvement of degradation by piezophoto- tronic catalysis over that by photocatalysis	[27]
$PbZr_{x}Ti_{1-x}O_{3}$ microspheres	stress induced by stirring	degradation of RhB (c=10 ppm)	$k = 0.012 \text{ min}^{-1}$	[13b]
NaNbO ₃ nanostructures	ultrasonic vibration + UV	degradation of MB $(c=32 \text{ mg L}^{-1})$	8% improvement in the incident-photon-to- current efficiency (IPCE) with ultrasonic vibration over that without	[19]
layered $\mathrm{Bi_4Ti_3O_{12}}$ few-layered $\mathrm{MoSe_2}$ nanoflowers	ultrasonic vibration ultrasonic vibration	degradation of MO degradation of RhB $(c=10 \text{ ppm})$	Over 80% decomposition within 6 h $k = 69889 \text{ ppm L mol}^{-1} \text{ s}^{-1}$	[20] [17]
$Bi_2O_2(OH)$ (NO ₃) nanosheets ZnO nanorods	ultrasonic vibration ultrasonic vibration	evolution of OH degradation of AO7 $(c=2 \text{ mg L}^{-1})$	7.13 mol L ⁻¹ min ⁻¹ for OH ca. 80% decomposition after 50 min	[21] [16b]

[a] k represents the pseudo-first-order rate constant.

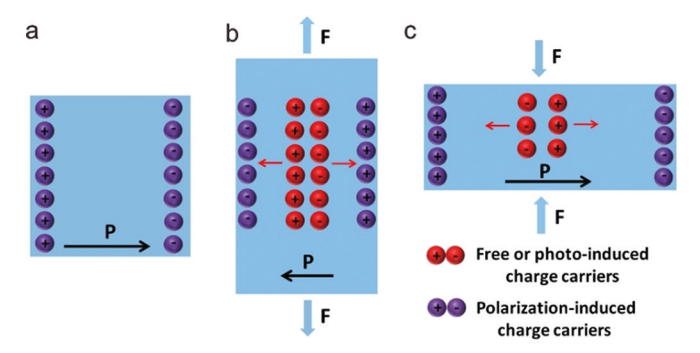


Figure 5. Pyroelectric materials a) in the absence of strain and under b) tension and c) compression.

dichlorofluorescin (DCF) suggested the formation of reactive oxygen species (ROS, i.e., hydroxyl radicals). [36] Barium

strontium titanate (Ba_{1-x}Sr_xTiO₃, BST) is a superior pyroelectric material. At x = 0.30, the highest pyroelectric effect of BST was reached, [37] exhibiting a pyroelectric coefficient of $8 \text{ nCcm}^{-1} \text{K}^{-1}$. The pyroelectric currents of BST (x = 0.3) nanoparticles were 2.8, 3.0, and 4.0 nA under the temperature differences of 0.10, 0.20, and 0.45 K, respectively (Figure 6eg).^[30] Owing to the increasing number of polarized carriers, the electrochemical impedance decreased as the temperature fluctuations increased (Figure 6h).^[30] The amount of hydrogen generated reached $46.89 \ \mu mol \, g^{-1}$ after $36 \ thermal \ cycles$ from 298 to 323 K. [30] Moreover, the puckered 2D few-layer black phosphorene exhibits approximately 99 % degradation of RhB after 5 cold-hot cycles from 288 to 338 K, and a direct hydrogen evolution of 540 μmol g⁻¹ catalysts after 24 thermal cycles.[34] More examples of pyroelectric catalysis are summarized in Table 2.





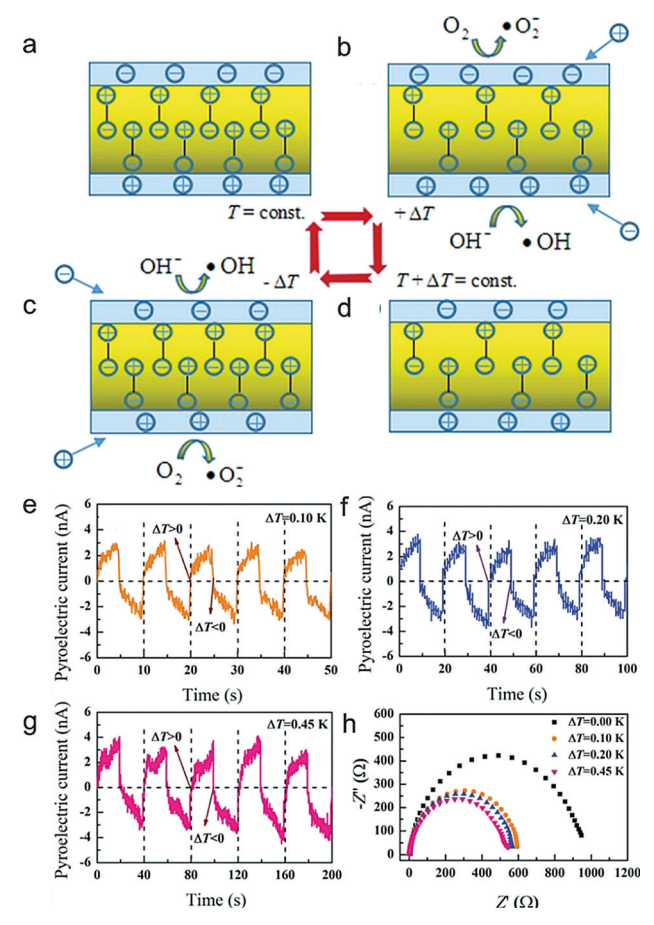


Figure 6. a–d) Schematic of the mechanism of pyro-catalysis. Adapted with permission from Ref. [29]. Copyright 2016, Royal Society of Chemistry. Pyroelectric currents of $Ba_{1-x}Sr_xTiO_3$ (BST; x=0.3) under the temperature fluctuations of e) 0.10 K, f) 0.20 K, and g) 0.45 K. h) Electrochemical impedance spectra (EIS) of BST (x=3) at varied temperature fluctuations. (e–h) Adapted with permission from Ref. [30]. Copyright 2018, Royal Society of Chemistry.

4. Ferroelectric-Material-Mediated Catalysis

Ferroelectric materials possess a similar polarization performance with and without strain to pyroelectric materials (Figure 5). Ferroelectric materials have polarization in the absence of strain. However, the polarization direction can be reversed by the application of external mechanical force. Apart from the strain and thermal excitation, the application

of an external electric field (i.e., poling) allows the manipulation of the spontaneous electric polarization.

Altman et al. demonstrated the ferroelectric-domaindependent adsorption of 2-propanol on separately poled, cand c⁺-oriented LiNbO₃ surfaces.^[39] After that, Li et al. reported the direct observation of ferroelectric-domaindependent physisorption energies using identical surfaces poled in situ. [40] AFM and scanning surface potential microscopy (SSPM) were employed to investigate the adsorption of CO_2 on $BaTiO_3$ (001) and $Pb(Zr_{0.48}Ti_{0.52})O_3$ (PZT) film.^[40] Prior to the CO₂ exposure, two close BaTiO₃ (Figure 7a) and PZT (Figure 7e) thin films were poled to have c⁺ domain (dark area) and c⁻ domain (bright area). The surface potential remained unchanged under CO₂ exposure up to 500 L. The change in surface potential (Figure 7b and Figure 7f, respectively) was ascribed to the chemisorption mediated by defects induced under vacuum annealing. [40] Under various CO2 doses, the surface potential of both c+ and c- domains decreased linearly with the increasing dose and then became almost invariant when the saturation coverage of CO₂ was approached (Figure 7c and Figure 7g, respectively).^[40] As the experiments (Figure 7c and Figure 7g) were carried out at room temperature and in situ poling did not change the concentration of defects, the different tendency (i.e., y axis) was caused by the difference of CO₂ coverage at constant exposure dose and the surface potential on the two opposite polarizations affected by adsorbed CO₂ variation. [40] As the chemisorption was influenced by defects, the saturation coverage was low and the neighboring adsorbates did not interact, the surface potential was linearly proportional to physical coverage of CO₂. [40] The reactive sticking coefficient S, defined as the ratio of impinging molecules that finally become chemisorbed, is shown in Equation (2):

$$\frac{\theta(L)}{\theta_{\rm max}} = \frac{V(L) - V(0)}{V_{\rm max} - V(0)} = \frac{SL}{\theta_{\rm max} N_0 \sqrt{2\pi m k_{\rm B} T}} \tag{2} \label{eq:delta_max}$$

where the coverage θ is the fraction of sites per unit area (i.e., N_0) that are occupied. For an ideal gas with exposure dose L, $\frac{L}{\sqrt{2\pi m k_B T}}$ refers to the number of impinging molecules. Figure 7 d and Figure 7 h depict that the dose dependencies of the potential were linear in a significant range with the ratios of the c⁻ to c⁺ slopes of 3.7 for BaTiO₃ and 2.5 for PZT, respectively. These results indicated that S is polarization dependent and invariable for a wide range of coverage and dose. A0

Table 2: Comparison of the catalytic performance among various pyrocatalytic semiconductors.

nanostructured semiconductors	external sources	catalytic applications	catalytic performance	Ref.
NaNbO₃ nanorods	heating-cooling cycles (321-348 K, 5 min)	degradation of RhB ($c=5 \text{ mg L}^{-1}$)	RhB completely decomposed after 24 cycles	[33]
$Ba_{0.7}Sr_{0.3}TiO_3$ nanoparticles	heating-cooling cycles (298-323 K, 10 min)	hydrogen evolution	Hydrogen evolution achieved 46.89 µmol g ⁻¹ after 36 cycles	[30]
BiFeO ₃ nanoparticles	heating-cooling cycles (300-311 K)	degradation of RhB ($c = 5 \text{ mg L}^{-1}$)	RhB almost totally degraded after ca. 200 cycles	[29]
2D few-layered black phosphorene	heating-cooling cycles (288-338 K)	(i) hydrogen evolution	(i) Hydrogen evolution reached 540 μmol g ⁻¹ after 24 cycles	[34]
	,	(ii) degradation of RhB ($c = 5 \text{ mg L}^{-1}$)	(ii) Approximately 99% RhB degraded after 5 cycles	





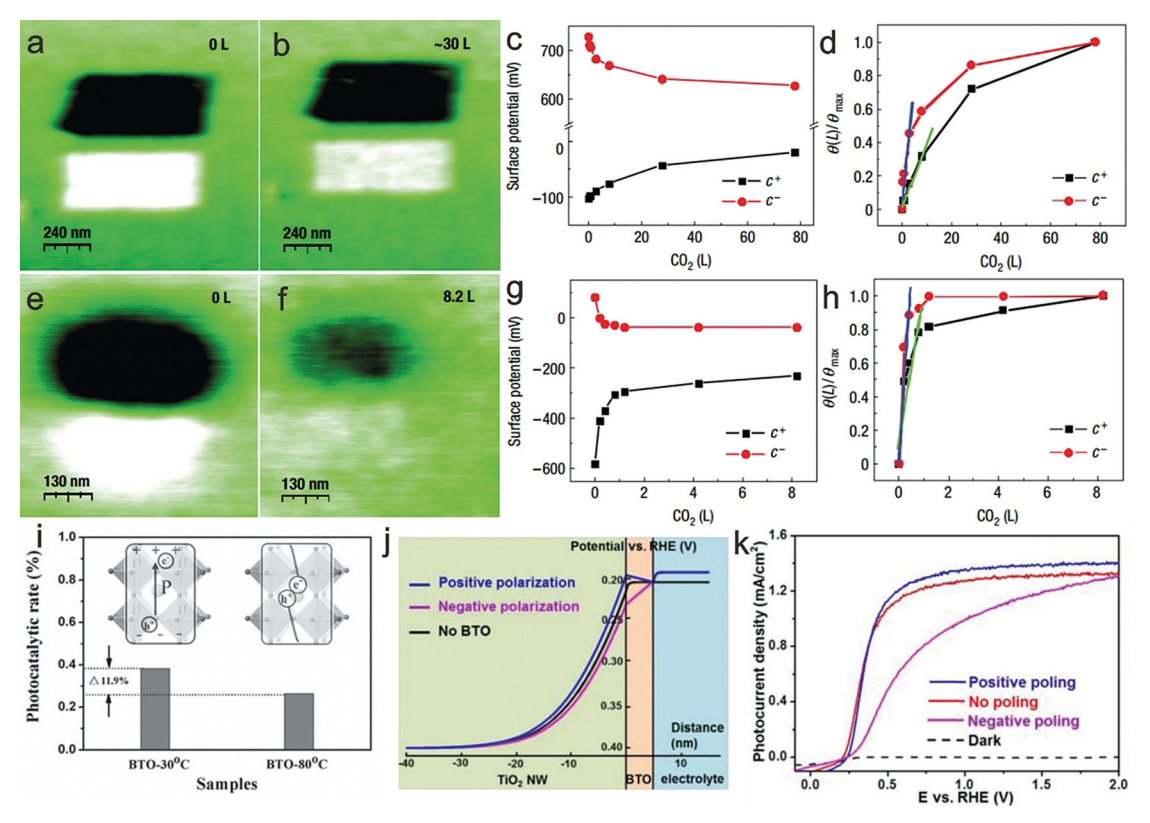


Figure 7. Surface potential maps of c^+ domain (dark area) and c^- domain (bright area) on BaTiO $_3$ (001) after exposure to a) 0 L and b) 30 L of CO $_2$. c) Average surface potential versus CO $_2$ dose on BaTiO $_3$ (001). d) $\theta(L)/\theta_{max}$ versus CO $_2$ dose of BaTiO $_3$ (001). (e–h) The corresponding results for CO $_2$ adsorption on PZT thin film as those in (a,b). (a–h) Adapted with permission from Ref. [40]. Copyright 2008, Nature Publishing Group. i) The photocatalytic degradation rate of RhB using BaTiO $_3$ nanoparticles as catalysts at 30 °C and 80 °C for 40 min. Adapted with permission from Ref. [41]. Copyright 2015, Wiley. j) Calculated potential distribution of TiO $_2$ (obtained at 150 °C)/BaTiO $_3$ (5 nm)/NaOH heterojunction. k) I–V curves of as-synthesized (red), positively poled (blue) and negatively poled (purple) TiO $_2$ (obtained at 150 °C)/BaTiO $_3$ (5 nm) nanowires. j,k) Adapted with permission from Ref. [42]. Copyright 2015, American Chemical Society.

It is worth noting that the ferroelectric effect was experimentally found to directly influence the photocatalytic performance. [41] The crystal structure of BaTiO₃ nanoparticles varied when the catalytic reaction was performed at different temperatures (i.e., 30°C and 80°C), leading to the different polarization of BaTiO₃. [41] As the polarization of BaTiO₃ nanoparticles at 80°C declined compared with that at 30°C, the photocatalytic decolorization of RhB decreased approximately 12% when temperature raised from 30°C to 80°C (Figure 7i). [41] Additionally, the polarization on BaTiO₃ film improved the band bending of TiO₂ nanowire arrays (Figure 7j) and thus increased the charge separation efficiency, resulting in the enhanced photocurrent density (Figure 7k). [42] Recently, KNbO₃ particles were synthesized and polarized for

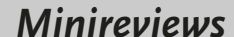
photocatalytic decomposition of RhB.^[43] Compared with unpolarized KNbO₃ counterpart, KNbO₃ particles displayed remarkable enhancement of photocatalytic performance, which can be attributed to the internal electric field after poling as evidenced by the longer photoluminescence lifetime.^[43] More examples of ferroelectric catalysis are presented in Table 3.

5. Summary and Outlook

In summary, PIEZOelectric semiconductors (i.e., piezoelectric, pyroelectric, and ferroelectric materials) have emerged as promising catalysts for a range of applications,

Table 3: Comparison of the catalytic performance among various ferrocatalytic semiconductors.

nanostructured semicon- ductors	external sources	catalytic applications	catalytic performance	Ref.
BaTiO ₃ nanoparticles	spontaneous polarization $+$ UV	degradation of RhB $(c=10 \text{ ppm})$	with spontaneous polarization at 30°C, 11.9% improvement in RhB degradation rate over that without spontaneous polarization at 80°C	[41]
KNbO ₃ particles	polarized by a customized polarizing device $+$ UV	degradation of RhB $(c=10 \text{ mg L}^{-1})$	$k = 0.317 \text{ min}^{-1}$	[43]







including the degradation of environmentally relevant organic pollutants, water splitting, and CO₂ reduction. Upon the implementation of external stress and strain, temperature variation, and electric field, these PIEZOelectric semiconductor nanomaterials experience the separation of positive and negative charge centers, that is, polarization, thereby creating an internal electric filed and in turn leading to highly efficient spatial separation of free charge carriers or photogenerated charge carriers. The spatial separation of charge carriers not only reduces the recombination between electrons and holes but also decreases the probability of reverse reactions between the oxidized and reduced products. As a result, the catalytic performance of this intriguing class of materials is enhanced owing to their PIEZOelectric effects (i.e., piezoelectric, pyroelectric, and ferroelectric effects), as exemplified in the effective degradation of a wide range of organic pollutants and hydrogen generation in this Minireview.

The advantages and disadvantages of the three PIEZOelectric semiconductors are briefly compared as follows. Compared to pyroelectric and piezoelectric catalysis, ferroelectric catalysis can be triggered by an external electric field, temperature variation, and mechanical force. In contrast, pyroelectric catalysis can be initiated by temperature changes and mechanical force, and piezoelectric catalysis can only be excited by mechanical force. Additionally, pyroelectrics and ferroelectrics possess dipoles even without an external trigger (Figure 5). In other words, pyroelectrics and ferroelectrics can slightly increase the separation of photo-generated electrons and holes in the absence of a trigger. However, piezoelectric materials that are not pyro or ferroelectric only show spontaneous polarization, that is they exhibit improved charge separation, under mechanical force (Figure 2). One of the main disadvantages for PIEZOcatalysts is that the external trigger, such as heat or mechanical force, should be changed from time to time. Otherwise the internal polarized electric field will be screened. For example, if the surrounding temperature remains the same, the polarized carriers can be totally screened by the carriers from the electrolyte after the thermodynamic equilibrium is reached between the pyroelectrics and the electrolyte (Figure 6a).[29] Similarly, the polarization-induced internal electric field of piezoelectric materials can also be screened if the external mechanical force exerted on piezoelectric catalysts does not change. [6]

Despite the impressive advantages of PIEZOelectric effect peculiar to PIEZOelectric semiconductors that enable PIEZOpotential for enhanced catalytic activities, there are issues that remain to be solved as well as exciting opportunities to further improve the PIEZOcatalytic efficiency.

First, more attention should be directed toward the specific PIEZOcatalytic mechanism. For example, in recent investigation into pyrocatalysis, polarized carriers were considered to participate the catalytic redox reactions. However, more studies should be conducted to corroborate the validity of this mechanism as free carriers or photo-generated carriers that are effectively separated by the built-in electric field owing to polarized carriers are highly likely to drive catalytic redox reactions. This merits a detailed exploration.

Second, it is greatly desirable to produce single-crystalline PIEZOelectric catalyst nanomaterials. This is because in polycrystalline catalysts, different domains may possess different polarization directions, thereby affecting the PIEZOpotentials of one another and resulting in weakened polarization-induced potential. Many techniques can be utilized to fabricate single-crystal materials, including the solution method, [44] aerosol chemical vapor deposition (ACVD), [45] the floating zone technique, [46] and hydrothermal reaction. [47] Moreover, the smaller the PIEZOelectric catalyst is in the polarization direction, the more easily free or photogenerated carriers will reach the active sites at the surface of catalysts driven by the internal electric field.

Third, ultrasonic waves have been recognized as an effective means of initiating the catalytic reaction. It is well-known that ultrasonic wave can increase the defects on the surface of materials. According to some reports, defects favor the separation of electron-hole pairs and play an important role in determining the kinetics, energetics, and catalytic mechanism. Therefore, intensive studies are needed to identify what is the main reason accounting for the improved catalytic efficiency during the ultrasonic process, that is, either the internal electric field caused by the piezopential or the increased defects generated.

Fourth, the PIEZOelectric effect can be readily extended to other applications, such as catalytic CO₂ reduction and nitrogen fixation. Enhanced carrier separation as a result of the polarization is expected to enable a drastically improved catalytic performance. In addition, for the normal catalytic process, another problem that limits the catalytic activity is the correlation among the binding energies of catalysts, reactants, intermediates, and products (described as the scaling relationship), which follows the Sabatier principle. It is notable that the interaction between catalysts and adsorbates is neither too weak to hinder the adsorption of reactants onto the surface of catalysts nor too strong to prohibit the desorption of products from the surface of catalysts. Periodic stress applied on the catalysts favors the adsorption and desorption processes of reactants and products, respectively, mediated by the periodic polarization.^[8]

Finally, other forms of clean energy, including wind, tidal, and geothermal energy, can also be exploited as energy sources to trigger the PIEZOcatalysis. Wind and tide can be utilized to apply stress on catalysts, while geothermal energy can be employed as the heat source to change the temperature of catalysts. As such, a greater progress in the wide spectrum of practical utilization of PIEZOcatalysts will be facilitated.

We hope this Minireview will serve as a useful reference and bring some inspiration in the design and investigation of both PIEZOcatalysts and the related PIEZOcatalytic mechanisms and procedures. Looking forward to the future of this exciting field, new challenges may continue to emerge and in turn create many opportunities for crafting a suite of new PIEZOcatalysts and effectively capitalizing on them for enhanced PIEZOcatalysis.

Minireviews





Acknowledgements

M.W. gratefully acknowledges the support from Sun Yat-Sen University. Z.L. gratefully acknowledges the support from the National Science Foundation (CMMI 1562075 and DMR 1709420). F.H. acknowledges the financial support from Major Research plan of the National Natural Science Foundation of China (No. 91833301, 61427901, and U1505252), the Science and Technology Program of Guangzhou, China (No. 201607020036).

Conflict of interest

The authors declare no conflict of interest.

How to cite: Angew. Chem. Int. Ed. **2019**, 58, 7526–7536 Angew. Chem. **2019**, 131, 7606–7616

- [1] M. Y. Wang, J. Ioccozia, L. Sun, C. J. Lin, Z. Q. Lin, Energy Environ. Sci. 2014, 7, 2182–2202.
- [2] a) M. Y. Wang, M. D. Ye, J. Iocozzia, C. J. Lin, Z. Q. Lin, Adv. Sci. 2016, 3, 1600024; b) M.-Q. Yang, L. Shen, Y. Lu, S. W. Chee, X. Lu, X. Chi, Z. Chen, Q.-H. Xu, U. Mirsaidov, G. W. Ho, Angew. Chem. Int. Ed. 2018, https://doi.org/10.1002/anie. 201810694; Angew. Chem. 2018, https://doi.org/10.1002/ange. 201810694; c) M.-Q. Yang, J. Dan, S. J. Pennycook, X. Lu, H. Zhu, Q.-H. Xu, H. J. Fan, G. W. Ho, Mater. Horiz. 2017, 4, 885–894; d) M.-Q. Yang, Y.-J. Xu, W. Lu, K. Zeng, H. Zhu, Q.-H. Xu, G. W. Ho, Nat. Commun. 2017, 8, 14224.
- [3] a) M. Y. Wang, X. C. Pang, D. J. Zheng, Y. J. He, L. Sun, C. J. Lin, Z. Q. Lin, J. Mater. Chem. A 2016, 4, 7190-7199; b) M. Y. Wang, L. Sun, Z. Q. Lin, J. H. Cai, K. P. Xie, C. J. Lin, Energy Environ. Sci. 2013, 6, 1211-1220; c) M. Wang, L. Sun, J. Cai, P. Huang, Y. Su, C. Lin, J. Mater. Chem. A 2013, 1, 12082-12087.
- [4] M. B. Starr, X. D. Wang, Nano Energy 2015, 14, 296-311.
- [5] G. Caserta, T. Cervigni, Proc. Natl. Acad. Sci. USA 1974, 71, 4421–4424.
- [6] H. Li, Y. Sang, S. Chang, X. Huang, Y. Zhang, R. Yang, H. Jiang, H. Liu, Z. L. Wang, *Nano Lett.* 2015, 15, 2372–2379.
- [7] J. L. Giocondi, G. S. Rohrer, J. Phys. Chem. B 2001, 105, 8275–8277.
- [8] A. Kakekhani, S. Ismail-Beigi, *J. Mater. Chem. A* **2016**, *4*, 5235 –
- [9] J. Shi, M. B. Starr, H. Xiang, Y. Hara, M. A. Anderson, J. H. Seo, Z. Q. Ma, X. D. Wang, *Nano Lett.* **2011**, *11*, 5587 – 5593.
- [10] M. B. Starr, J. Shi, X. Wang, Angew. Chem. Int. Ed. 2012, 51, 5962-5966; Angew. Chem. 2012, 124, 6064-6068.
- [11] a) K. S. Hong, H. F. Xu, H. Konishi, X. C. Li, J. Phys. Chem. Lett.
 2010, I, 997-1002; b) K. S. Hong, H. F. Xu, H. Konishi, X. C. Li, J. Phys. Chem. C 2012, 116, 13045-13051; c) Y. F. Cui, J. Briscoe, S. Dunn, Chem. Mater. 2013, 25, 4215-4223; d) S. Y. Lan, J. X. Feng, Y. Xiong, S. H. Tian, S. W. Liu, L. J. Kong, Environ. Sci. Technol. 2017, 51, 6560-6569; e) L. L. Zhao, Y. Zhang, F. L. Wang, S. C. Hu, X. N. Wang, B. J. Ma, H. Liu, Z. L. Wang, Y. H. Sang, Nano Energy 2017, 39, 461-469; f) J. Wu, N. Qin, D. H. Bao, Nano Energy 2018, 45, 44-51.
- [12] a) C. F. Tan, W. L. Ong, G. W. Ho, Acs Nano 2015, 9, 7661 7670;
 b) X. Y. Xue, W. L. Zang, P. Deng, Q. Wang, L. L. Xing, Y. Zhang, Z. L. Wang, Nano Energy 2015, 13, 414 422;
 c) X. Guo, Y. M. Fu, D. Y. Hong, B. W. Yu, H. X. He, Q. Wang, L. L. Xing, X. Y. Xue, Nanotechnology 2016, 27, 375704;
 d) D. Y. Hong, W. L. Zang, X. Guo, Y. M. Fu, H. X. He, J. Sun, L. L. Xing, B. D. Liu, X. Y. Xue, ACS Appl. Mater. Interfaces 2016, 8, 21302 21314;
 e) L. F. Wang, S. H. Liu, Z. Wang, Y. L. Zhou, Y. Qin,

Angew. Chem. Int. Ed. 2019, 58, 7526-7536

- Z. L. Wang, *Acs Nano* **2016**, *10*, 2636 2643; f) K. Q. Wang, Z. B. Fang, X. Y. Huang, W. H. Feng, Y. Z. Wang, B. Wang, P. Liu, *Chem. Commun.* **2017**, *53*, 9765 9768.
- [13] a) H. Lin, Z. Wu, Y. M. Jia, W. J. Li, R. K. Zheng, H. S. Luo, Appl. Phys. Lett. 2014, 104, 162907; b) Y. W. Feng, L. L. Ling, Y. X. Wang, Z. M. Xu, F. L. Cao, H. X. Li, Z. F. Bian, Nano Energy 2017, 40, 481–486.
- [14] M. K. Lo, S. Y. Lee, K. S. Chang, J. Phys. Chem. C 2015, 119, 5218–5224.
- [15] M. B. Starr, X. D. Wang, Sci. Rep. 2013, 3, 2160.
- [16] a) J. M. Wu, W. E. Chang, Y. T. Chang, C. K. Chang, Adv. Mater. 2016, 28, 3718–3725; b) J. M. Wu, Y. G. Sun, W. E. Chang, J. T. Lee, Nano Energy 2018, 46, 372–382.
- [17] M. H. Wu, J. T. Lee, Y. J. Chung, M. Srinivaas, J. M. Wu, Nano Energy 2017, 40, 369-375.
- [18] H. W. Huang, S. C. Tu, C. Zeng, T. R. Zhang, A. H. Reshak, Y. H. Zhang, Angew. Chem. Int. Ed. 2017, 56, 11860-11864; Angew. Chem. 2017, 129, 12022-12026.
- [19] S. Singh, N. Khare, Nano Energy 2017, 38, 335-341.
- [20] S. C. Tu, H. W. Huang, T. R. Zhang, Y. H. Zhanga, Appl. Catal. B 2017, 219, 550-562.
- [21] L. Hao, H. W. Huang, Y. X. Guo, Y. H. Zhang, ACS Sustainable Chem. Eng. 2018, 6, 1848–1862.
- [22] X. L. Xu, Y. M. Jia, L. B. Xiao, Z. Wu, Chemosphere 2018, 193, 1143–1148.
- [23] X. Wang, Nano Energy 2012, 1, 13-24.
- [24] E. B. Flint, K. S. Suslick, Science 1991, 253, 1397-1399.
- [25] C. Sun, Y. M. Fu, Q. Wang, L. L. Xing, B. D. Liu, X. Y. Xue, RSC Adv. 2016, 6, 87446–87453.
- [26] Y. T. Wang, K. S. Chang, J. Am. Ceram. Soc. 2016, 99, 2593– 2600.
- [27] B. Y. Dai, L. Zhang, H. M. Huang, C. H. Lu, J. H. Kou, Z. Z. Xu, Appl. Surf. Sci. 2017, 403, 9–14.
- [28] Z. L. Wang, Nano Today 2010, 5, 540-552.
- [29] J. Wu, W. J. Mao, Z. Wu, X. L. Xu, H. L. You, A. X. Xue, Y. M. Jia, *Nanoscale* 2016, 8, 7343 7350.
- [30] X. Xu, L. Xiao, Y. Jia, Z. Wu, F. Wang, Y. Wang, N. O. Haugen, H. Huang, *Energy Environ. Sci.* 2018, 2018, 11, 2198–2207.
- [31] Y. Yang, W. X. Guo, K. C. Pradel, G. Zhu, Y. S. Zhou, Y. Zhang, Y. F. Hu, L. Lin, Z. L. Wang, *Nano Lett.* 2012, 12, 2833 – 2838.
- [32] a) H. D. Espinosa, R. A. Bernal, M. Minary-Jolandan, *Adv. Mater.* 2012, 24, 4656–4675; b) M. Minary-Jolandan, R. A. Bernal, I. Kujanishvili, V. Parpoil, H. D. Espinosa, *Nano Lett.* 2012, 12, 970–976; c) A. N. Morozovska, E. A. Eliseev, G. S. Svechnikov, S. V. Kalinin, *J. Appl. Phys.* 2010, 108, 042009.
- [33] H. L. You, Z. Wu, L. Wang, Y. M. Jia, S. Li, J. Zou, Chemosphere 2018, 199, 531 – 537.
- [34] H. You, Y. Jia, Z. Wu, F. Wang, H. Huang, Y. Wang, Nat. Commun. 2018, 9, 2889.
- [35] A. Benke, E. Mehner, M. Rosenkranz, E. Dmitrieva, T. Leisegang, H. Stocker, W. Pompe, D. C. Meyer, J. Phys. Chem. C 2015, 119, 18278–18286.
- [36] E. Gutmann, A. Benke, K. Gerth, H. Bottcher, E. Mehner, C. Klein, U. Krause-Buchholz, U. Bergmann, W. Pompe, D. C. Meyer, J. Phys. Chem. C 2012, 116, 5383-5393.
- [37] A. Ianculescu, I. Pintilie, C. A. Vasilescu, M. Botea, A. Iuga, A. Melinescu, N. Dragan, L. Pintilie, Ceram. Int. 2016, 42, 10338–10348.
- [38] G. Z. Zhang, S. L. Jiang, Y. K. Zeng, Y. Y. Zhang, Q. F. Zhang, Y. Yu, J. Wang, *Phys. Status Solidi A* 2011, 208, 2699 2708.
- [39] Y. Yun, E. I. Altman, J. Am. Chem. Soc. 2007, 129, 15684 15689.
- [40] D. B. Li, M. H. Zhao, J. Garra, A. M. Kolpak, A. M. Rappe, D. A. Bonnell, J. M. Vohs, *Nat. Mater.* 2008, 7, 473–477.
- [41] S. Ran, S. Yajing, L. Linglong, Z. Dawei, Y. Guang, G. Chuanbo, Y. Yaodong, *Small* 2015, 11, 202 – 207.
- [42] W. G. Yang, Y. H. Yu, M. B. Starr, X. Yin, Z. D. Li, A. Kvit, S. F. Wang, P. Zhao, X. D. Wang, Nano Lett. 2015, 15, 7574-7580.

Minireviews





- [43] Q. Fu, X. J. Wang, C. Y. Li, Y. Sui, Y. P. Han, Z. Lv, B. Song, P. Xu, RSC Adv. 2016, 6, 108883–108887.
- [44] a) Z. Zhang, Y. Zhu, W. Wang, W. Zheng, R. Lin, F. Huang, J. Mater. Chem. C 2018, 6, 446–451; b) Y. Bi, S. Ouyang, N. Umezawa, J. Cao, J. Ye, J. Am. Chem. Soc. 2011, 133, 6490–6492.
- [45] W.-N. Wang, W.-J. An, B. Ramalingam, S. Mukherjee, D. M. Niedzwiedzki, S. Gangopadhyay, P. Biswas, J. Am. Chem. Soc. 2012, 134, 11276–11281.
- [46] A. J. E. Rettie, H. C. Lee, L. G. Marshall, J. F. Lin, C. Capan, J. Lindemuth, J. S. McCloy, J. S. Zhou, A. J. Bard, C. B. Mullins, J. Am. Chem. Soc. 2013, 135, 11389 11396.
- [47] a) J. Shao, W. Sheng, M. Wang, S. Li, J. Chen, Y. Zhang, S. Cao, Appl. Catal. B 2017, 209, 311 – 319; b) J. Li, W. Zhao, F. Huang, A. Manivannan, N. Wu, Nanoscale 2011, 3, 5103 – 5109.
- [48] a) X. C. Jiao, Z. W. Chen, X. D. Li, Y. F. Sun, S. Gao, W. S. Yan, C. M. Wang, Q. Zhang, Y. Lin, Y. Luo, Y. Xie, J. Am. Chem. Soc. 2017, 139, 7586-7594; b) L. Hao, L. Jie, A. Zhihui, J. Falong, Z. Lizhi, Angew. Chem. Int. Ed. 2018, 57, 122-138; Angew. Chem. 2018, 130, 128-145.

Manuscript received: October 11, 2018 Revised manuscript received: November 24, 2018 Accepted manuscript online: December 16, 2018 Version of record online: March 26, 2019